Molecular Actuators Designed with S∴N(sp^2) Hemibonds Attached to a Conformationally Flexible Pivot

Yong-Hui Tian and Miklos Kertesz*

Department of Chemistry, Georgetown University, 37th & O Street, Washington, D.C. 20057-1227

Received January 6, 2009. Revised Manuscript Received March 18, 2009

We propose an electromechanical actuator based on the electroactive hinge, 2-(2-(methylsulfanyl)phenyl)pyridine (MSPPy, **3**), in which the formation of 2c/3e S∴N(sp^2) hemibonds generate the driving forces for the molecular motion of the biphenyl-like pivot. The expansion and contraction of the molecular configuration are controlled by the formation and dissociation of the hemibonds at the neutral and +1 oxidized state of the molecule, respectively. The structural and electronic properties of the proposed actuators are characterized through density functional theory (DFT) and ab initio calculations. Several analogous molecules are carefully analyzed in order to validate the presented theoretical approach. The formation of an intramolecular S∴N(sp^2) hemibond in the radical cation of MSPPy ($\mathbf{3}^{\bullet+}$) is supported by the short S···N distance, significant Mayer's bond order indices, and the characteristic stretching frequencies. The S∴N(sp^2) bonding strength is estimated using the conformational method. A further improvement of the nanoactuator is anticipated by turning off the noncovalent C−S···N interactions in neutral MSPPy (**3**) by introducing an appropriately located methyl group.

Introduction

The design of molecular machines has been an intriguing challenge for chemists to mimic actions of biological motors.[1] One of the most interesting subjects is to develop actuators or artificial muscles, which simulate some aspect of the contractions associated with skeletal muscles. Various actuation mechanisms are based on the ability of the actuator materials or assemblies to transduce optical,[2] electrical,[3] or chemical[4] stimulus into mechanical work through dimensional response. The advantages and limitations of the reported artificial muscles have been summarized by Baughman, and strategies to improve the performance were suggested.[5]

Electroactive materials that attracted much interest as electromechanical actuators include conducting polymers such as polypyrrole,[6] polyaniline,[7] and polythiophene[8] and helical structures.[9] The operating principle of this class of redox-active materials is based on the intercalation of dopants and counterions by inducing a volume change of the polymer matrix by swelling. The major disadvantage of this bulk mechanism is that the actuation frequency is diffusion limited by the counterion flux. To overcome this limitation, researchers have discovered alternatives where the actuation mechanism relies on the intrinsic properties of the actuator materials as e.g. for polyacetylene and carbon nanotubes.[10] The linear strain (s) is defined as the ratio of the change (Δl) to the length (l) of polymer chains or nanotube sheets as a function of injected charge (q):

$$s(q) = \Delta l(q)/l \quad (1)$$

For the intrinsic mechanism, s is small because the dimensional change in this case is due to the contraction or

* Corresponding author. E-mail: kertesz@georgetown.edu.

(1) Kottas, G. S.; Clarke, L. I.; Horinek, D.; Michl, J. *Chem. Rev.* **2005**, *105*, 1281.
(2) (a) Brouwer, A. M.; Frochot, C.; Gatti, F. G.; Leigh, D. A.; Mottier, L.; Paolucci, F.; Roffia, S.; Wurpel, G. W. H. *Science* **2001**, *291*, 2124. (b) Mateo-Alonso, A.; Guldi, D. M.; Paolucci, F.; Prato, M. *Angew. Chem., Int. Ed.* **2007**, *46*, 8120. (c) Altieri, A.; Bottari, G.; Dehez, F.; Leigh, D. A.; Wong, J. K. Y.; Zerbetto, F. *Angew. Chem., Int. Ed.* **2003**, *42*, 2296. (d) Ballardini, R.; Balzani, V.; Gandolfi, M. T.; Prodi, L.; Venturi, M.; Philp, D.; Ricketts, H. G.; Stoddart, J. F. *Angew. Chem., Int. Ed.* **1993**, *32*, 1301. (e) Muraoka, T.; Kinbara, K.; Aida, T. *Nature (London)* **2006**, *440*, 512.
(3) (a) Saha, S.; Flood, A. H.; Stoddart, J. F.; Impellizzeri, S.; Silvi, S.; Venturi, M.; Credi, A. *J. Am. Chem. Soc.* **2007**, *129*, 12159. (b) Sobransingh, D.; Kaifer, A. E. *Org. Lett.* **2006**, *8*, 3247. (c) Altieri, A.; Gatti, F. G.; Kay, E. R.; Leigh, D. A.; Paolucci, F.; Slawin, A. M. Z.; Wong, J. K. Y. *J. Am. Chem. Soc.* **2003**, *125*, 8644.
(4) (a) Badjic, J. D.; Balzani, V.; Credi, A.; Silvi, S.; Stoddart, J. F. *Science,* **2004**, *303*, 1845. (b) Fletcher, S. P.; Dumur, F.; Pollard, M. M.; Feringa, B. L. *Science* **2005**, *310*, 80. (c) Badjic, J. D.; Ronconi, C. M.; Stoddart, J. F.; Balzani, V.; Silvi, S.; Credi, A. *J. Am. Chem. Soc.* **2006**, *128*, 1489. (d) Marlin, D. S.; Cabrera, D. G.; Leigh, D. A.; Slawin, A. M. Z. *Angew. Chem., Int. Ed.* **2006**, *45*, 77. (e) Ebron, V. H.; Yang, Z. W.; Seyer, D. J.; Kozlov, M. E.; Oh, J. Y.; Xie, H.; Razal, J.; Hall, L. J.; Ferraris, J. P.; MacDiarmid, A. G.; Baughman, R. H. *Science* **2006**, *311*, 1580.
(5) Baughman, R. H. *Science* **2005**, *308*, 63.
(6) (a) Otero, T. F.; Cortes, M. T. *Adv. Mater.* **2003**, *15*, 279. (b) Deshpande, S. D.; Kim, J.; Yun, S. R. *Synth. Met.* **2005**, *149*, 53. (c) Ding, J.; Zhou, D.; Spinks, G.; Wallace, G.; Forsyth, S.; Forsyth, M.; MacFarlane, D. *Chem. Mater.* **2003**, *15*, 2392. (d) Lin, X.; Li, J.; Elisabeth, S.; Yip, S. *Int. J. Quantum Chem.* **2005**, *102*, 980.
(7) (a) Smela, E.; Mattes, B. R. *Synth. Met.* **2005**, *151*, 43. (b) Smela, E.; Lu, W.; Mattes, B. R. *Synth. Met.* **2005**, *151*, 25. (c) Kaneto, K.; Kanekoa, M.; Minb, Y.; MacDiarmid, A. G. *Synth. Met.* **1995**, *71*, 2211. (d) Baughman, R. H. *Synth. Met.* **1996**, *78*, 339.
(8) (a) Han, G. Y.; Shi, G. Q. *Sens. Actuators, B* **2004**, *99*, 525. (b) Lu, W.; Fadeev, A. G.; Qi, B. H.; Smela, E.; Mattes, B. R.; Ding, J.; Spinks, G. M.; Mazurkiewicz, J.; Zhou, D. Z.; Wallace, G. G.; MacFarlane, D. R.; Forsyth, S. A.; Forsyth, M. *Science* **2002**, *297*, 983.
(9) Rempala, P.; King, B. T. *J. Chem. Theory Comput.* **2006**, *2*, 1112.
(10) Sun, G.; Kurti, J.; Kertesz, M. *J. Chem. Phys.* **2002**, *117*, 7691. (b) Baughman, R. H.; Cui, C. X.; Zakhidov, A. A.; Iqbal, Z.; Barisci, J. N.; Spinks, G. M.; Wallace, G. G.; Mazzoldi, A.; De Rossi, D.; Rinzler, A. G.; Jaschinski, O.; Roth, S.; Kertesz, M. *Science* **1999**, *284*, 1340. (c) Sun, G. Y.; Kurti, J.; Kertesz, M.; Baughman, R. H. *J. Am. Chem. Soc.* **2002**, *124*, 15076.

10.1021/cm900029z CCC: $40.75
Published on Web 04/27/2009

Chart 1. Schematic Drawing of the Proposed Actuator Composed of an Electroactive MSPPy (3) Pivot and Linear Rigid Beams (shaded); Shaded Rectangles Indicate the Attached Groups That Rotate Relative to One Another

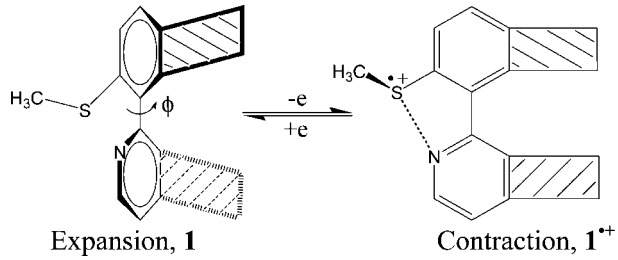

expansion of covalent bonds upon electrochemical reduction and oxidation. With this in mind, chemists are interested in constructing actuators driven by conformational changes at the molecular level. Promising systems include thiophene-fused [8]annulene,[11] π-stacking thiophene oligomers,[12] and crown-annelated oligothiophenes.[13] PVDF (poly-(vinylidene fluoride))-based nanoactuators have been investigated both experimentally[14] and computationally,[15] showing large lattice strains (experimentally often characterized by the percent change of film thickness) associated with phase transformations of the material. On the basis of a different mechanism rotaxane-based molecular shuttle-actuator is capable of reversible mechanical switching driven by chemical, electrochemical, or photochemical stimuli in solution.[16]

In this paper, we introduce a novel strategy to design molecular actuators based on a floppy biphenyl-like (2-phenylpyridine, 2PPy) pivot and redox-controlled S···N interactions. The proposed general architecture and actuation process is illustrated in Chart 1. The building block is composed of three components: an electroactive part, a movable rigid beam carrying the load (shaded in Chart 1) and a 2PPy pivot. The first two parts are bridged through the 2PPy pivot. The electroactive component and the 2PPy pivot are built of 2-(2-(methylsulfanyl)phenyl)pyridine (MSPPy, **3**) in our design. The divalent sulfur and the proximal sp^2 hybridized nitrogen in MSPPy (**3**) play the role of the electroactive component through the formation of a S∴N hemibond after a one-electron oxidation of the actuating unit which in turn results in the planarization of 2PPy, which transduces the forces into the rigid beams leading to a closed

Chart 2. Orbital Diagram for the 2c/3e $[H_2S\therefore SH_2]^{\bullet+}$ Hemibond

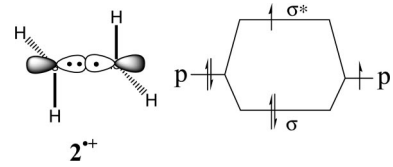

configuration as shown in Chart 1. It is well-known that divalent sulfur compounds can easily be one-electron oxidized, giving rise to radical cations essentially localized on sulfur because of the relatively low ionization potentials of these molecules.[17] The S-centered radical cations can be stabilized by a partner atom bearing an appropriately oriented electron lone pair allowing the formation of a two-center (2c), three-electron (3e) hemibond,[18,19] or $2\sigma/1\sigma^*$ bond, denoted as S∴X in this study (X is the atom providing lone pair electrons). 2c/3e hemibonds can be qualitatively described by the orbital diagram of the prototype $[H_2S\therefore SH_2]^{\bullet+}$ system as depicted in Chart 2.[20]

The two p-orbitals on sulfur, one bearing the cation radical and the other bearing the lone pair of a neutral molecule, overlap, resulting in one doubly occupied bonding orbital and one singly occupied antibonding orbital. Therefore, the cation radical is stabilized through mixed-valence bonding in the dimer. In an analogy to the prototypical hemibond in $[H_2S\therefore S\ H_2]^{\bullet+}$, in this study we propose an intramolecular S∴N(sp^2) hemibond in MSPPy ($\mathbf{3}^{\bullet+}$) that acts as an electroactive hinge.

The other feature of the proposed design is the flexibility of the $\alpha-\alpha'$ connection of the 2PPy scaffold, which acts as a pivot to transduce the forces generated by the formation of a S∴N hemibond to the rigid beams. It is well-known that biphenyl and analogous molecules are quite floppy with respect to the torsion angle along the bridging $C_\alpha-C_{\alpha'}$ bond.[21−23]

As is discussed in the following sections, the expected dimensional response of the designed actuators is high. In this study, the geometrical and electronic properties of the proposed molecular actuators are explored with density functional theory (DFT) and ab initio (MP2) calculations.

(11) Marsella, M. J.; Reid, R. J.; Eatassi, S.; Wang, L.-S. *J. Am. Chem. Soc.* **2002**, *124*, 12507.
(12) (a) Scherlis, D. A.; Marzari, N. *J. Am. Chem. Soc.* **2005**, *127*, 3207. (b) Yu, H.-h.; Xu, B.; Swager, T. M. *J. Am. Chem. Soc.* **2003**, *125*, 1142. (c) Takita, R.; Song, C.; Swager, T. M. *Org. Lett.* **2008**, *10*, 5003.
(13) Jousselme, B.; Blanchard, P.; Levillain, E.; Delaunay, J.; Allain, M.; Richomme, P.; Rondeau, D.; Gallego-Planas, N.; Roncali, J. *J. Am. Chem. Soc.* **2003**, *125*, 1363.
(14) Zhang, Q. M.; Bharti, V.; Zhao, X. *Science* **1998**, *280*, 2101.
(15) Strachan, A.; Goddard, W. A. *Appl. Phys. Lett.* **2005**, *86*, 083103.
(16) (a) Badjic, J. D.; Balzani, V.; Credi, A.; Silvi, S.; Stoddart, J. F. *Science* **2004**, *303*, 1845. (b) Liu, Y.; Flood, A. H.; Bonvallet, P. A.; Vignon, S. A.; Northrop, B. H.; Tseng, H.-R.; Jeppesen, J. O.; Huang, T. J.; Brough, B.; Baller, M.; Magonov, S.; Solares, S. D.; Goddard, W. A.; Ho, C.-M.; Stoddart, J. F. *J. Am. Chem. Soc.* **2005**, *127*, 9745. (c) Brough, B.; Northrop, B. H.; Schmidt, J. J.; Tseng, H.-R.; Houk, K. N.; Stoddart, J. F.; Ho, C.-M. *Proc. Natl. Acad. Sci. U.S.A.* **2006**, *103*, 8583.
(17) Bernardi, F.; Csizmadia, I. G.; Mangini, A. *Organic Sulfur Chemistry*; Elsevier: Amsterdam, 1985; p 486.
(18) (a) Gill, P.M. W.; Radom, L. *J. Am. Chem. Soc.* **1988**, *110*, 4931. (b) Gill, P.M. W.; Weatherall, P.; Radom, L. *J. Am. Chem. Soc.* **1989**, *111*, 2782. (c) Clark, T. *J. Comput. Chem.* **1982**, *3*, 112. (d) Clark, T. *J. Am. Chem. Soc.* **1988**, *110*, 1672. (e) Clark, T. *J. Comput. Chem.* **1981**, *2*, 261. (f) Illies, A. J.; Livant, P.; McKee, M. L. *J. Am. Chem. Soc.* **1988**, *110*, 7980. (g) James, M. A.; McKee, M. L.; Illies, A. J. *J. Am. Chem. Soc.* **1996**, *118*, 7836. (h) Fernández, P. F.; J. V.; Ortiz, J. V.; Walters, E. A. *J. Chem. Phys.* **1986**, *84*, 1653.
(19) Pauling, L. *J. Am. Chem. Soc.* **1931**, *53*, 3225.
(20) (a) Asmus, K. D. *Acc. Chem. Res.* **1979**, *12*, 436. (b) Asmus, K. D.; Bonifacic, M. In *Sulfur-Centered Radicals*; Alfassi, Z. B., Eds.; John Wiley & Son: New York, 1999; p 141.
(21) (a) Karpfen, A.; Choi, C. H.; Kertesz, M. *J. Phys. Chem. A* **1997**, *101*, 7426. (b) Grein, F. *J. Phys. Chem. A* **2002**, *106*, 3823. (c) Dobbs, K. D.; Sohlberg, K. *J. Chem. Theory Comput.* **2006**, *2*, 1530.
(22) Almenningen, A.; Bastiansen, O.; Fernholt, L.; Cyvin, B. N.; Cyvin, S. J.; Samdal, S. *J. Mol. Struct.* **1985**, *128*, 59.
(23) Sancho-Garcia, J. C.; Cornil, J. *J. Chem. Theory Comput.* **2005**, *1*, 581.

The performance of the theory level used in the paper is evaluated through comparisons with experiments whenever possible. The S∴N hemibond strength is compared to other well-studied 2c/3e hemibonds involving S-centered radical cations. The strategies to modify the 2PPy pivot are discussed in order to improve the performance of the proposed electrochemical actuators, including molecular springs composed of several electroactive units.

Computational Methodology

Full geometry optimizations[24] were carried out using the Becke's three-parameter (B3) hybrid exchange functionals combined with Lee−Yang−Parr (LYP) correlation functionals (B3LYP).[25] The performance of B3LYP for 2c/3e hemibonds has been evaluated showing good agreement with high level calculations including Møller−Plesset perturbation theory of the second order (MP2). [26] Moreover, the calculated $(N\therefore N)^{\bullet+}$ distance in **7** is in good agreement with the X-ray structure. On the other hand, a large number of theoretical studies on the 2c/3e S∴X systems have been reported using BH&HLYP functionals, which include half Hartree−Fock exchange, half Slater exchange, and a LYP correlation functional.[27] Therefore, we additionally used BH&HLYP for comparison with the B3LYP calculations. The fully optimized structures were examined by frequency calculations at the same theory level to confirm that they are local minima. We also use the hybrid meta-generalized gradient M05−2X functional,[28] which has been recently developed aiming to account for correlation energies at medium and long range. The performance of this functional has been evaluated for various systems including the difficult boron−nitrogen coordinate covalent bond strength,[29] closed-shell dimers,[30] and the energetics of bond dissociation.[31] Previous studies suggest that the hemibond energies and distances display little basis set dependence.[32] The effect of basis set on the optimized the geometric parameters are also evaluated in this study, indicating that the modest basis set of 6-31G(d) gives very similar results when compared with the larger basis sets such as 6-31G(2d,p). Therefore, all fully optimized geometries in this study are calculated using the 6-31G(d) basis set. As all of the hemibonding systems in this study were open shell ($S = 1/2$), we checked the spin contamination for the calculations with unrestricted (U) methods. The square of spin angular momentum is very close to the ideal value of 0.75 for all of the reported calculations with UB3LYP, UBH&HLYP, and UM05−2X methods. All potential energy scans (PESs) are fully relaxed unless specific constraints are explicitly stated.

Chart 3. Structures of the Neutral (3) and Oxidized ($3^{\bullet+}$) MSPPy and Its Conformer ($4^{\bullet+}$); The Latter Is Used for Bond Energy Analysis, See Text

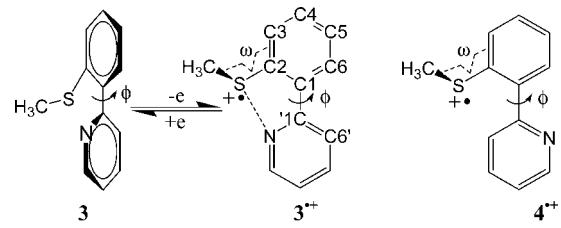

Natural bond orbital (NBO) analysis was performed by employing the NBO 3.1 program[33] for the evaluation of electron donor−acceptor interactions.

Mayer's bond order (MBO) analysis was performed using the program APEX4[34] based on the single determinant wave function built upon the Kohn−Sham orbitals in DFT. According to Mayer, the ab initio bond index between atom A and B can be defined as[35]

$$B_{AB} = 2\sum_{\mu\in A}\sum_{\nu\in B}[(P^{\alpha}S)_{\mu\nu}(P^{\alpha}S)_{\nu\mu} + (P^{\beta}S)_{\mu\nu}(P^{\beta}S)_{\nu\mu}] \quad (2)$$

where S is the overlap matrix; P^{α} and P^{β} are the density matrix for spin α and spin β, respectively.[36,37]

In addition to the bond order indices, we evaluated the strength of the intramolecular 2c/3e hemibonds by employing the conformational method,[38] which has been applied for evaluating the intramolecular hydrogen bonding energies.[39] In this study, the intramolecular bonding is switched on (structure $\mathbf{3}^{\bullet+}$) and off (structure $\mathbf{4}^{\bullet+}$) through the rotation around the bridging C1C1′ bond as shown in Chart 3. The 2c/3e hemibond energies are estimated by calculating the energy difference between $\mathbf{3}^{\bullet+}$ and its conformer $\mathbf{4}^{\bullet+}$. The electronic delocalization energy and steric repulsion might also contribute to the energy difference between the two conformations. However, such contributions are expected to be a minor factor compared to the 2c/3e hemibonds if, for the conformer $\mathbf{4}^{\bullet+}$, the dihedral angles (ω) between the H_3CS- group and the phenyl ring were constrained at the same values as that of the fully optimized geometry of structure $\mathbf{3}^{\bullet+}$. Detailed discussion is presented in the following sections. Three theory levels including B3LYP, MP2, and CCSD are used for the energy calculations of the isomers based on the geometries optimized at B3LYP/6-31G(d) level. The MP2 calculation is based on restricted Hartree−Fock reference orbitals (ROMP2).

(24) Frisch, M. J.; et al. *Gaussian 03, revision D.01*; Gaussian, Inc.: Pittsburgh, PA, 2003.
(25) (a) Becke, A. D. *J. Chem. Phys.* **1993**, *98*, 5648. (b) Lee, C.; Yang, W.; Parr, R. G. *Phys. Rev. B* **1988**, *37*, 785.
(26) (a) Carmichael, I. *Acta Chem. Scand.* **1997**, *51*, 567. (b) James, M. A.; McKee, M. L.; Illies, A. J. *J. Am. Chem. Soc.* **1996**, *118*, 7836. (c) Deng, Y.; Illies, A. J.; James, M. A.; McKee, M. L.; Peschke, M. *J. Am. Chem. Soc.* **1995**, *117*, 420.
(27) Becke, A. D. *J. Chem. Phys.* **1993**, *98*, 1372.
(28) (a) Zhao, Y.; Schultz, N. E.; Truhlar, D. G. *J. Chem. Theory Comput.* **2006**, *2*, 364. (b) Zhao, Y.; Truhlar, D. G. *Acc. Chem. Res.* **2008**, *41*, 157.
(29) Plumley, J. A.; Evanseck, J. D. *J. Chem. Theory Comput.* **2008**, *4*, 1249.
(30) Zhao, Y.; Truhlar, D. G. *J. Chem. Theory Comput.* **2007**, *3*, 289.
(31) (a) Wodrich, M. D.; Corminboeuf, C.; Schreiner, P. R.; Fokin, A. A.; Schleyer, P. v. R. *Org. Lett.* **2007**, *9*, 1851. (b) Rokob, T. A.; Hamza, A.; Papai, I. *Org. Lett.* **2007**, *9*, 4279.
(32) Braida, B.; Hiberty, P. C.; Savin, A. *J. Phys. Chem. A* **1998**, *102*, 7872.
(33) NBO Version 3.1, Glendening, E. D.; Reed, A. E.; Carpenter, J. E.; Weinhold, F.
(34) Mayer, I.; Hamza, A. *APEX4, version 1.0*; Hungarian Academy of Science: Budapest, Hungary, 2004.
(35) Mayer, 1. *Int. J. Quantum Chem.* **1986**, *29*, 73.
(36) Mayer, I. *J. Comput. Chem.* **2006**, *28*, 204.
(37) Mayer, I. *Simple Theorems, Proofs, and Derivations in Quantum Chemistry*, Kluwer Academic/Plenum Publishers: New York 2003, *241*.
(38) (a) George, P.; Trachtman, M.; Bock, C. W.; Brett, A. M. *Tetrahedron* **1976**, *32*, 317. (b) Hehre, W. J.; Radom, L.; Scheleyer, P. v. R.; Pople, J. A. *Ab Initio Molecular Orbital Theory*; John Wiley Sons: New York, 1986.
(39) (a) Kovacs, A.; Szabo, A.; Hargittai, I. *Acc. Chem. Res.* **2002**, *35*, 887. (b) Lampert, H.; Mikenda, W.; Karpfen, A. *J. Phys. Chem.* **1996**, *100*, 7418. (c) Kjaergaard, H. G.; Howard, D. L.; Schofield, D. P.; Robinson, T. W.; Ishiuchi, S.; Fujii, M. *J. Phys. Chem. A* **2002**, *106*, 258.

Chart 4. Structures of the Radical Cations of DTCO ($5^{\bullet+}$) and 3-MTPA ($6^{\bullet+}$)

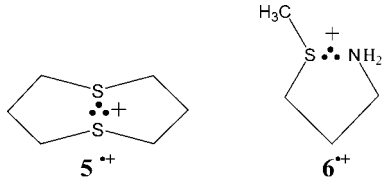

Results and Discussion

2c/3e S∴X hemibonds can be established not only between molecules but also within a molecule when cationic radical S-center interacts with a nearby atom (X) bearing an appropriate lone pair in the same molecule.[40] In accordance with the simple orbital overlap justification, the formation of S∴X hemibonds is favored for the molecular configurations which allow the alignment between the sulfur 3p orbital and the lone pair orbital on atom X. Two typical cases are shown in Chart 4: 1,5-dithiacycloocane[41] (DTCO, $\mathbf{5}^{\bullet+}$) and 3-methylthio propylamine[42] (3-MTPA, $\mathbf{6}^{\bullet+}$), both of which form strong 2c/3e hemibonds after one-electron oxidation. The relatively strong bonding manifests itself in the high stability of their radical salts as established by ESR measurements in acetonitrile solution[41b,43] as well as the low oxidation potentials measured by cyclic voltammetry in acetonitrile.[44] Moreover, intramolecular hemibonds are expected to be kinetically more stable compared to the intermolecular ones, because the molecular framework helps to hold the two atoms forming hemibond in proximity of each other. For instance, some intramolecular $(N\therefore N)^{+\bullet}$ hemibonds have been characterized by X-ray diffraction.[45] An example is shown in Chart 5, in which the $(N\therefore N)^{+\bullet}$ hemibond in *N*,*N*-trimethylene-syn-1,6:8,13-diimino[14]annulene ($\mathbf{7}^{\bullet+}$) has an unusual equilibrium N−N distance of 2.160 Å.[46]

Inspired by these examples, we suggest molecular actuators driven by the reversible formation and disassociation of S∴N hemibonds in a redox process. sp^3 hybridized nitrogen ($N(sp^3)$) provides a σ lone pair, as for example, NH_3. sp^2 hybridized nitrogen ($N(sp^2)$) can provide a σ lone pair, as for example, pyridine, or $N(sp^2)$ can be a π electron donor, as for example, in pyrrole. Our calculations indicate that NH_3 and pyridine forms a three electron hemibond with the S-centered radical cation of $H_2S^{\bullet+}$. As shown in Chart 6, the optimized S∴N hemibond distances are very similar for the two systems, $[H_3N\therefore SH_2]^{\bullet+}$ ($\mathbf{8}^{\bullet+}$) and $[C_5H_5N\therefore SH_2]^{\bullet+}$ ($\mathbf{9}^{\bullet+}$). In this study, we classify the S∴N hemibonds into two types: $S\therefore N(sp^3)$ and $S\therefore N(sp^2)$. These are illustrated as $\mathbf{8}^{\bullet+}$ and $\mathbf{9}^{\bullet+}$ in Chart 6. As will be seen in the following sections, the hemibonds involved in the design of actuators belong to the $S\therefore N(sp^2)$ type.

Chart 5. Structure of the Radical Cation of *N*,*N*-trimethylene-*syn*-1,6:8,13-diimino[14]annulene[46] (CSD refcode: DULDAP)

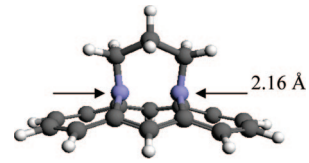

($7^{\bullet+}$)

Chart 6. Optimized Geometries of $[H_3N\therefore SH_2]^{\bullet+}$ ($8^{\bullet+}$) and $[C_5H_5N\therefore SH_2]^{+\bullet}$ ($9^{\bullet+}$) at the B3LYP/6-31G(d) Level

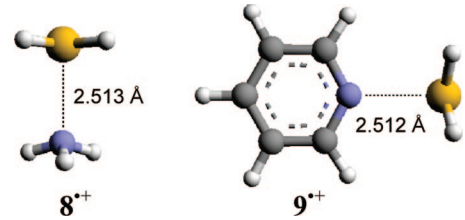

Table 1. Calculated Torsion Angles ϕ (deg) (see Chart 3 for the labeling) in the MSPPy (3) and MTTPPy (11) Hinge in the Neutral and One-Electron Oxidized State; The 6-31G(d) Basis Set Is Used for All Calculations

	MSPPy (**3**)		MMTPPy (**11**)	
oxidation state	**3**	$\mathbf{3}^{\bullet+}$	**11**	$\mathbf{11}^{\bullet+}$
B3LYP	36.29	2.18	56.70	1.44
BH&HLYP	40.93	1.72	58.34	1.45
M05−2X	40.98	1.50	55.93	0.85

S∴N(sp^2) Hemibond in the Oxidized MSPPy ($3^{\bullet+}$) and C−S···N Noncovalent Bonding in the Neutral State (3). For the MSPPy hinge (**3**), the torsion angle ϕ (C6−C1−C1′−C6′) along the bridging C1−C1′ bond (see Chart 3 for the labeling) is the characteristic geometry parameter related to the molecular motion in a redox actuation process. As shown in Table 1, the fully geometry optimization with different DFTs indicates that the dihedral angles are around 40° at the neutral state (**3**) because of steric repulsions, whereas in the one-electron oxidized state ($\mathbf{3}^{\bullet+}$), the configuration becomes nearly planar. Therefore, the MSPPy (**3**) hinge is electroactive with respect to the rotations along the C1−C1′ bond of the 2PPy pivot.

According to the fully optimized geometries with various DFTs, the radical cation of MSPPy ($\mathbf{3}^{\bullet+}$) shows that ϕ is close to zero (see Table 1) and the S···N distance of 2.411 Å is far below the sum of van der Waals radii of sulfur and nitrogen. These geometrical characteristics clearly indicate that an intramolecular $S\therefore N(sp^2)$ hemibond has been formed.

(40) (a) Momose, T.; Suzuki, T.; Shida, T. *Chem. Phys. Lett.* **1984**, *107*, 568. (b) Asmus, K. D.; Gillis, H. A.; Teather, G. G. *J. Phys. Chem.* **1978**, *82*, 2677. (c) Asmus, K. D.; Bahnemann, D.; Fischer, C. H.; Veltwisch, D. *J. Am. Chem. Soc.* **1979**, *101*, 5322.
(41) (a) Musker, W. K.; Wolford, T. L. *J. Am. Chem. Soc.* **1976**, *98*, 3055. (b) Musker, W. K.; Wolford, T. L.; Roush, B. P. *J. Chem. Soc.* **1978**, *100*, 6416.
(42) Tripathi, G. N. R.; Tobien, T. *J. Phys. Chem. A* **2001**, *105*, 3498.
(43) Musker, W. K. *Acc. Chem. Res.* **1980**, *13*, 200.
(44) (a) Wilson, G. S.; Swanson, D. D.; Klug, J. T.; Glass, R. S.; Ryan, M. D.; Musker, W. K. *J. Am. Chem. Soc.* **1979**, *101*, 1040. (b) Block, E.; Glass, R. S.; DeOrazio, R.; Lichtenberger, D. L.; Pollard, J. R.; Russell, E. E.; Schroeder, T. B.; Thiruvazhi, M.; Toscano, P. J. *Synlett* **1997**, 525.
(45) (a) Alder, R. W.; Orpen, A. G.; White, J. M. *J. Chem. Soc., Chem. Commun.* **1985**, 949. (b) Gerson, F.; Gescheidt, G.; Buser, U.; Vogel, E.; Lex, J.; Zehnder, M.; Reisen, A. *Angew. Chem., Int. Ed. Engl.* **1989**, *28*, 902.
(46) Gerson, F.; Knobel, J.; Buser, U.; Vogel, E.; Zehnder, M. *J. Am. Chem. Soc.* **1986**, *108*, 3781.

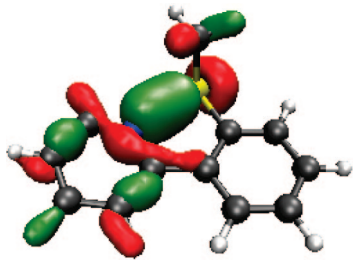

Figure 1. Bonding molecular orbital of the hemibond (corresponds to the σ orbital in Chart 2) of S:.N(sp^2) in the radical cation of MSPPy (**3**$^{\bullet+}$) at the B3LYP/6-31G(d) level.

The molecular orbital (see Figure 1) displays strong bonding overlap between the sulfur and the nitrogen. Additionally, the Mulliken atomic spin density is 98% localized on sulfur and nitrogen, further indicating that the S∴N(sp^2) hemibond is localized between the sulfur and the nitrogen.

We also calculated the Mayer's bond order (MBO) to characterize the strength of the S∴N(sp^2) hemibond. Bridgeman et al. have applied the MBO index to characterize the bond strength for both the two center chemical bonds and multicenter bonding including the weak S···S bonding in the S_4N_4 cage. [47] The MBO index for the intramolecular S∴N(sp^2) hemibond in MSPPy (**3**$^{\bullet+}$) is listed in Table 2. In order to assess the strength of the intramolecular S∴N(sp^2) hemibonds, the bond orders of several typical N∴N (**7**$^{\bullet+}$), S∴S(**5**$^{\bullet+}$, **10**$^{\bullet+}$) and S∴N(sp^3) (**6**$^{\bullet+}$) hemibonds were also provided. The formation of the $Me_2S∴SMe_2$ dimer (**10**$^{\bullet+}$) has been experimentally confirmed by mass spectroscopy.[48]

The bond order indices indicate that the strength of the S∴N(*sp*^{2}) hemibond in MSPPy (**3**$^{\bullet+}$) is comparable to that of the typical S∴N(*sp*^{3}) hemibond in 3-MTPA (**6**$^{\bullet+}$), and it is a somewhat weaker than the symmetric S∴S hemibonds are in $Me_2S∴SMe_2^{\bullet+}$ (**10**$^{\bullet+}$) and DTCO (**5**$^{\bullet+}$). The vibrational frequencies dominated by the S∴X stretching vibrations are also listed for the radical cations of these compounds in Table 2. The calculated unscaled frequency is in fair agreement with the experimental value for 3-MTPA (**6**$^{\bullet+}$). The similar wavenumbers further indicate that the bond strengths of the S∴N(sp^2) hemibond in MSPPy (**3**$^{\bullet+}$) are comparable to the typical S∴N(sp^3) hemibond in 3-MTPA (**6**$^{\bullet+}$). The calculated slightly larger wavenumber for **7**$^{\bullet+}$ is due to the coupling of the N∴N stretching with vibrations of the attached framework. As shown in Table 2, the calculated N∴N distance for **7**$^{\bullet+}$ is in good agreement with the X-ray structure, further confirming the reliability of this level of theory for these systems. The calculated S···N distance in MSPPy (**3**$^{\bullet+}$) is a little longer than that in 3-MTPA (**6**$^{\bullet+}$). All the above evidence indicate that the S∴N(sp^2) hemibond in MSPPy (**3**$^{\bullet+}$) is relatively strong and is capable of providing the driving forces for the planarization of the 2PPy pivot.

We evaluated the S∴N(sp^2) bonding energies using the conformational method described in the methodology section. The main structural difference between MSPPy (**3**$^{\bullet+}$) and the conformer (**4**$^{\bullet+}$) is that for the later, the H_3CS- group is positioned far away from the nitrogen heteroatom preventing the formation of an S∴N(sp^2) hemibond. Second, the delocalization energies are different for the two systems. The fully optimized geometry of the conformer (**4**$^{\bullet+}$) indicates that the dihedral angle ω tends to be zero (see Chart 3 for the labeling and Figure 2S in the Supporting Information for the fully optimized geometry). This is because such planarization favors electron delocalization between the S(3p) orbitals and the π molecular orbitals on the phenyl ring. However, for MSSPy (**3**$^{\bullet+}$), there is a competing effect of forming a S∴N(sp^2) hemibond, which favors the dihedral angle of 90° and reduces the electron delocalization. To evaluate the strength of S∴N(sp^2) hemibonds using the conformational method, we should keep the delocalization effect at the same level for MSPPy (**3**$^{\bullet+}$) and the conformer (**4**$^{\bullet+}$). For this reason, the geometries of the conformer (**4**$^{\bullet+}$) were optimized with the dihedral angle ω, constrained to the same value of the MSPPy (**3**$^{\bullet+}$) (See Figure 3S in the Supporting Information for the fully optimized geometry for **3**$^{\bullet+}$ and the constrained geometry for **4**$^{\bullet+}$), and the total energies were calculated based on the constrained geometry. In this construction, the energy difference between **3**$^{\bullet+}$and **4**$^{\bullet+}$ mainly arises from the presence and absence of a hemibond, respectively. The estimated S∴N(sp^2) bonding energies thus calculated are listed in Table 3 using the B3LYP and ROMP2 and CCSD methods. All these various theory levels give a strong bonding interaction which is in accordance to the large MBO indices obtained for **3**$^{\bullet+}$.

For an efficient molecular actuator, the electroactive components should not be too flexible with respect to the characteristic geometry parameters, such as the torsion angle ϕ in this study. Otherwise, the actuating function would be lost when the actuator is working against a load. Therefore, we examined the potential energy surface of MSPPy (**3**$^{\bullet+}$) in the one-electron oxidized state. The relevant PES is presented in Figure 2 which shows a barrier of ~10 kcal/mol at $\phi = 90°$.

We now turn to the electronic and structural properties of the neutral MSPPy (**3**) molecule. The noncovalent bonding interactions between divalent sulfur and heteroatoms like oxygen and nitrogen have been recognized in many organic compounds.[49] Such noncovalent interactions are schematically described as X−S···Y, where X is covalently boned to S. The formation of the noncovalent X−S···Y contact is generally attributed to the donation of the electrons from the highest occupied π or n orbitals of Y to the unoccupied σ^* orbitals of the S−X bonds.[50] Inspecting the fully optimized geometry of neutral MSPPy (**3**), we find a number of geometric indicators for the existence of noncovalent C−S···

(47) Bridgeman, A. J.; Cavigliasso, G.; Ireland, L. R.; Rothery, J. *J. Chem. Soc., Dalton Trans.* **2001**, 2095.
(48) (a) Illies, A. J.; Nichols, L. S.; James, M. A. *J. Am. Mass Spectrom.* **1997**, *8*, 605. (b) Visser, S. P.; Bickelhaupt, F. M.; Koning, L. J.; Nibbering, N. M. M. *Int. J. Mass Spectrom.* **1998**, *179*, 43.
(49) (a) Iwaoka, M.; Takemoto, S.; Okada, M.; Tomoda, S. *Bull. Chem. Soc. Jpn.* **2002**, *75*, 1611. (b) Iwaoka, M.; Komatsu, H.; Katsuda, T.; Tomoda, S. *J. Am. Chem. Soc.* **2002**, *124*, 1902. (c) Minkin, V. I.; Minyaev, R. M. *Chem. Rev.* **2001**, *101*, 1247.
(50) (a) Gurm Row, T. N.; Parthasarathy, R. *J. Am. Chem. Soc.* **1981**, *103*, 477. (b) Roy, D.; Sunoj, R. B. *J. Phys. Chem. A* **2006**, *110*, 5942. (c) Iwaoka, M.; Katsuda, T.; Komatsu, H.; Tomoda, S. *J. Org. Chem.* **2005**, *70*, 321. (d) Ozen, A. S.; Atilgan, C.; Sonmez, G. *J. Phys. Chem. C* **2007**, *111*, 16362. (e) Rosenfield, R. E.; Parthasarathy, R.; Dunitz, J. D. *J. Am. Chem. Soc.* **1977**, *99*, 4860.

Table 2. Mayer's Bond Order (MBO) Indices, Stretching Frequencies (cm^{-1}), and Bond Distances (Å) of Some S∴S, S∴N, N∴N, and S∴N Hemibonds in This Study; Numbers in Parentheses Correspond to Experimental Values; All Calculations Were Done at the B3LYP/6-31G(d) Level

	$10^{\bullet+}$ $Me_2S\therefore SMe_2$	$7^{\bullet+}$	$5^{\bullet+}$ DTCO	$6^{\bullet+}$ 3-MTPA	$3^{\bullet+}$MSPPy
type of contact	S∴S	N∴N	S∴S	S∴N(sp^3)	S∴N(sp^2)
MBO	0.4255	0.3022	0.4343	0.3793	0.3648
stretching frequency	229	399/481[a]	222	265 (288)[b]	296
r(S∴S), *r*(S∴N), or r(N∴N)	2.946	2.190 (2.160)[c]	2.844	2.574 (∼2.50)[b]	2.411

[a] The N∴N stretching modes strongly couple with other vibrations. [b] See ref 42. [c] See ref 46.

Table 3. S∴N(sp^2) Bonding Energies (kcal/mol) in the Radical Cation of MSPPy ($3^{\bullet+}$) Approximated by the Energy Difference between $3^{\bullet+}$ and $4^{\bullet+}$; Geometries for the Energy Calculations Are All Optimized at the B3LYP/6-31G(d) level; Dihedral Angle ω of $4^{\bullet+}$ is Constrained to the Same Value As That in $3^{\bullet+}$

	B3LYP/6-31G(d)	ROMP2/6-31G (d, p)	CCSD/cc-pVDZ
$E(4^{\bullet+})-E(3^{\bullet+})$	17.73	18.51	22.39

N interactions, as shown in Table 4. First, the S···N distance is 2.86 Å, far below the sum of van de Waals radii of sulfur and nitrogen. Second, the H_3CS- group is nearly coplanar with the attached phenyl ring, which allows the alignment between the lone pair orbital of nitrogen and the unoccupied σ^* orbital of the S−C bond leading to donor−acceptor interactions between S and N. The small value of MBO index also indicates the presence of weak C−S···N interactions. The NBO method has been widely used for the noncovalent bonding analysis involving donor−acceptor interactions. The extent of noncovalent interactions can be described with the second-order perturbative stabilization energies, $E(2)$.[51] The calculated $E(2)$ is 2.76 kcal/mol (see Table 4), which is consistent with the non-negligible bond order index. The C−S···N interactions tends to counteract the steric repulsion and reduce the characteristic dihedral angle of the MSPPy hinge at the neutral state (**3**), which might impair the magnitude of dimensional change. To increase the dimensional response, we further modified the MSPPy (**3**) hinge aiming for a more open molecular shape in the neural state, as discussed in the following section.

Electronic and Structural Properties of Neutral (11) and Oxidized ($11^{\bullet+}$) 2-(3-Methyl-2-(methylthio)phenyl)pyridine. To switch off the nonbonded C−S···N interactions aiming for a more open configuration in the neutral state, we suggest a further modification of MSPPy (**3**) by introducing a methyl group ortho to the H_3CS- group. This modified hinge leads to MMTPPy (**11**), which is illustrated in Figure 3.

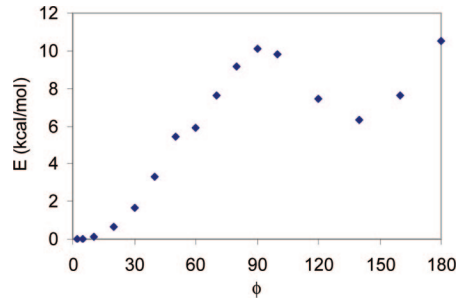

Figure 2. Potential energy scan of the radical cation of MSPPy ($3^{\bullet+}$) at the B3LYP/6-31G(d) level. The scanning is along the torsion angle ϕ (deg).

Table 4. Geometrical Parameters, MBO Indices, and Interaction Energy $E(2)$ between S and N in Neutral MSPPy (3) and Neutral MMTPPy (11) Calculated at the B3LYP/6-31G(d) Level; See Chart 3 for the Atomic Labeling

	S···N (Å)	Me−S−C2−C3 (ω) (deg)	C6−C1−C1′−C6′ (ϕ) (deg)	MBO	$E(2)$ (kcal/mol)
MSPPy (**3**)	2.86	22.02	36.29	0.07	2.76
MTTPPy (**11**)	3.27	93.05	56.70	0.01	<0.50

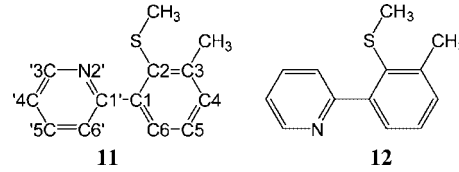

Figure 3. Chemical structures of MMTPPy (**11**) and its conformer (**12**).

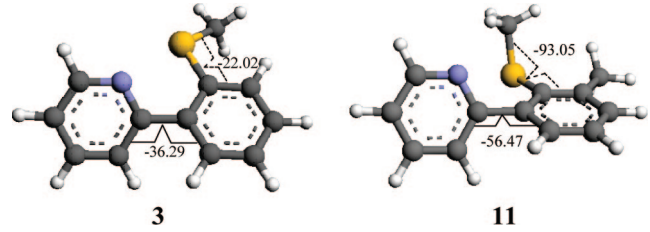

Figure 4. Fully optimized geometry of (a) neutral MSPPy (**3**) and (b) neutral MMTPPy (**11**). Dashed line, the dihedral angle of Me−S−C2−C3 (ω); solid line, the dihedral angle of C6−C1−C1′−C6′ (ϕ). The calculations are at the B3LYP/6-31G(d) level.

According to the fully optimized geometry (See Table 4), the torsion angle of the neutral MMTPPy (**11**) is 56.70°, significantly larger than that of the neutral MSPPy (**3**). Accordingly, MMTPPy (**11**) is expected to be more efficient as an actuating molecule. For the neutral MSPPy (**3**), as shown in Figure 4a, N, S−C are nearly aligned, which allows the C−S···N interactions. For the neutral MMTPPy (**11**), however, the steric repulsion between the two methyl groups prevents the alignment of N, and S−C as shown in Figure 4b. As a result, the noncovalent C−S···N interactions are impeded, and the neutral MMTPPy (**11**) is more open than neutral MSPPy (**3**). The disappearance of C−S···N interactions in neutral MMTPPy (**11**) is further confirmed by the negligible S···N MBO index and interaction energy, $E(2)$, as shown in Table 4.

The function of the methyl group as an inhibitor of the nonbonded C−S···N interaction is also reflected by comparing the potential energy surfaces of MSPPy (**3**) and MMTPPy (**11**) as shown in Figure 5. Because of the prevention of C−S···N interactions and the large steric repulsion between the lone pair of sulfur and nitrogen, MMTPPy (**11**) displays a much higher barrier than MSPPy (**3**) with respect to the planar configuration.

(51) Weinhold, F.; Landis, C. R. *Valency and Bonding: A Natural Bond Orbital Donor−Acceptor Perspective*; Cambridge University Press: New York, 2005; p 16.

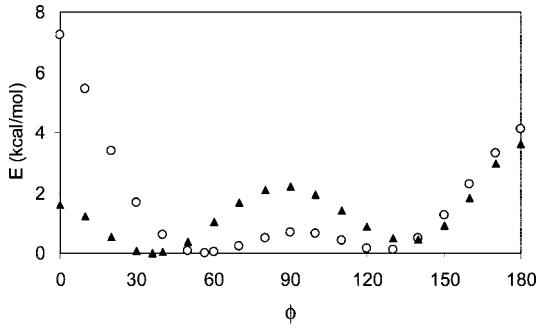

Figure 5. Potential energy scan as a function of ϕ (deg) of the neutral MSPPy (**3**, triangles) and neutral MMTPPy (**11**, open circles) at the B3LYP/6-31G(d) level.

Table 5. S∴N(sp²) Bonding Energies (kcal/mol) in MMTPPy ($11^{\bullet+}$) Estimated by the Conformational Method As the Energy Difference between $11^{\bullet+}$ and $12^{\bullet+}$; Geometries for Energy Calculations Are All Optimized at the B3LYP/6-31G(d) Level; Dihedral Angle ω of $12^{\bullet+}$ is Constrained to the Same Value as that in $11^{\bullet+}$

method	B3LYP/6-31G(d)	ROMP2/6-31G(d, p)
$E(\mathbf{12}^{\bullet+})-E(\mathbf{11}^{\bullet+})$	17.68	18.74

In the one-electron oxidized state, a S∴N(sp²) hemibond forms, and the MMTPPy ($\mathbf{11}^{\bullet+}$) hinge is planarized just as for MSPPy ($\mathbf{3}^{\bullet+}$). The strength of this S∴N(sp²) hemibond can be approximately evaluated with the conformational method using the isomer shown by $\mathbf{12}^{\bullet+}$ in Figure 3 The estimated S∴N(sp²) energies at the B3LYP and ROMP2 level are listed in Table 5. The calculated hemibonding energies are very close to the corresponding values of MSPPy ($\mathbf{3}^{\bullet+}$). However, as shown in Figure 6, the potential surface of MMTPPy ($\mathbf{11}^{\bullet+}$) shows an energy barrier of 14.5 kcal/mol, which is significantly larger than 10.1 kcal/mol of MSPPy ($\mathbf{3}^{\bullet+}$). Therefore, the MMTPPy ($\mathbf{11}^{\bullet+}$) is more rigid than MSPPy ($\mathbf{3}^{\bullet+}$) in their one-electron oxidized state. A possible reason for that is that as shown in Figure 7, at the torsion angle of 90°, the steric repulsion between the two methyl groups prevent effective electron delocalization between the sulfur and the attached phenyl ring for MMTPPy ($\mathbf{11}^{\bullet+}$).

Actuation Simulation. With the finding that MMTPPy (**11**) is more dimensionally sensitive than MSPPy (**3**) in a redox process, we build molecular actuators based on the rotational motion of this electroactive hinge, and simulate the actuation behavior of the proposed actuators. For this purpose, we add "loading beams" to MMTPPy (**11**) such that the proposed actuators act like a cantilever driven by

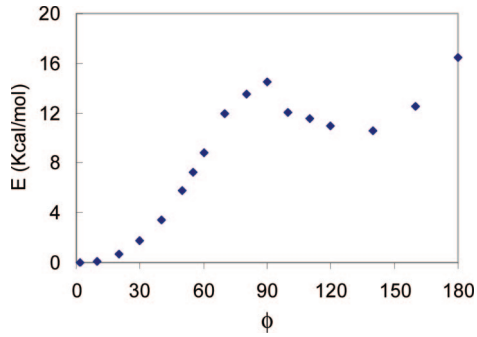

Figure 6. Potential energy scan of MMTPPy ($\mathbf{11}^{\bullet+}$) as a function of the dihedral angle ϕ along the C1−C1′ bond at the B3LYP/6-31G(d) level.

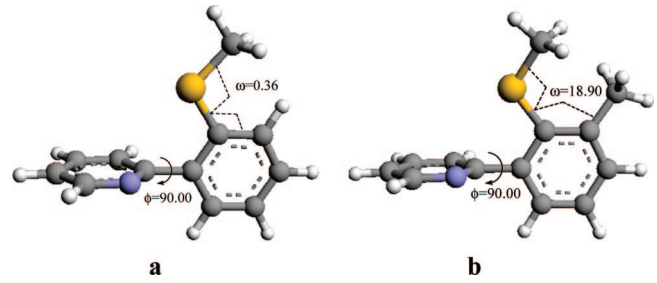

Figure 7. Optimized geometries of (a) MSPPy ($\mathbf{3}^{\bullet+}$); (b) MMTPPy ($\mathbf{11}^{\bullet+}$) with the constraint of $\phi = 90°$ at the B3LYP/6-31G(d) level. The optimized dihedral angle is given in degrees.

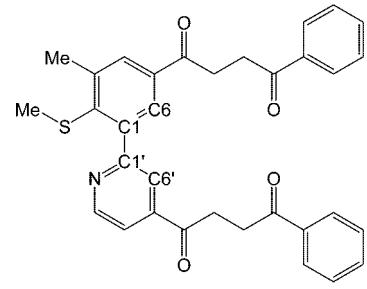

Figure 8. Structure of the proposed actuators based on MMTPPy (**11**).

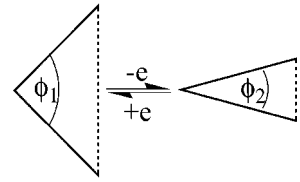

Figure 9. Schematic diagram illustrating the variables in eq 3.

forces associated with the formation and disassociation of S∴N(sp²) hemibonds in a redox process. Two criteria are suggested for the selection of the appropriate beams: (i) the beams should be rigid, and (ii) the electroactive property of the MMTPPy (**11**) hinge should remain intact after it is connected to the beams. In this study, the actuators (**13**) are constructed as sketched in Figure 8 for the actuation simulation. The dimensional response of the actuator can be described with the openness of the two beams as illustrated in Figure 9. The strain (s) is the percentage change of the length of the molecular assembly which is approximately equal to

$$s = \frac{\left(\sin\frac{\phi_2}{2} - \sin\frac{\phi_1}{2}\right)}{\sin\frac{\phi_1}{2}} \times 100\% \qquad (3)$$

Where ϕ_1, ϕ_2 are the C6−C1−C1′−C6′ torsion angles of the MMTPPy (**11**) hinge in the neutral and charged state, respectively.

According to the simulation results shown in Figure 10, the torsion angles change from 57.07° at the neutral state (**13**) to 6.53° in the one-electron oxidized state ($\mathbf{13}^{\bullet+}$), and the strain without the load is around 88% as obtained from eq 3. This dimensional response is quite large compared to the electrochemical actuators reported earlier. More importantly, the electroactive property of the MMTPPy (**11**) hinge remains intact after the connection with the

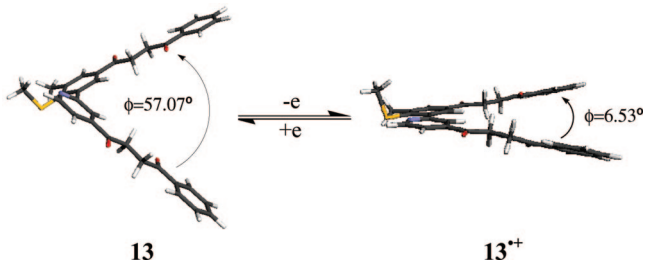

Figure 10. Open (reduced) and closed (oxidized) configurations of the proposed actuator (**13**) optimized at the B3LYP/6-31G(d) level.

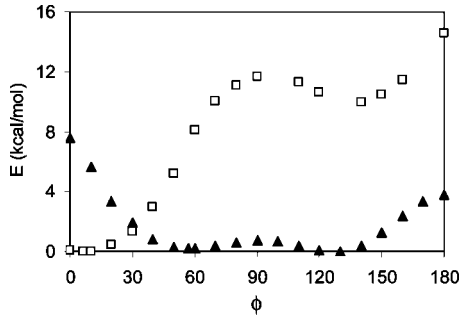

Figure 11. Potential energy scan of **13** (triangles) and **13**$^{\bullet+}$ (open squares). The scanning is along the torsion angle ϕ at the B3LYP/6-31G(d) level.

extended beams. As seen from Figure 11, in the neutral and the one-electron oxidation state, the actuator (**13**) shows very similar potential energy surfaces as MMTPPy (**11**). This further indicates that the electronic properties of MMTPPy (**11**) are not affected by the beams. Under "push" load, the structure is expected to be below but close to the minimum at $\phi = 60°$. Upon oxidation the molecule will slide to $\phi = 0°$. This motion is reversible and it is our model of actuation under "push" load. Under "pull" load, the structure is expected to be above but close to the minimum at $\phi = 125°$. Upon oxidation, the molecule will remain close to this configuration and no actuation would result, unless the angle is under $\phi = 90°$. This might be achievable with conformational restrictions. In that case, the system would slide down to $\phi = 0°$, also reversibly.

The actuators **13** shown in Figure 10 can be extended by introducing an additional electroactive unit of the MMTPPy (**11**) hinge on the other side of the beams as shown by the structure **14** in Figure 12. As the electroactive properties of the MMTPPy (**11**) hinge remain intact after being connected to the extended arms, each MMTPPy (**11**) can be envisioned as an isolated electroactive unit. Thus, a molecular spring can be built up with an array of the electroactive units connected with extended beams. Each unit is expected to work independently but in unison with respect to the response to the electrical stimulus, and thus they jointly contribute to the contraction or expansion of the molecular spring. We performed a quantum mechanical simulation at the B3LYP/6-31G(d) level for the actuator (**14**) composed of two MMTPPy hinges and three beams as shown in Figure 12. The optimized structures are illustrated in Figure 12 for the neutral state (**14**) and the two-electron oxidized state (**14**$^{2+}$), respectively. As expected, the electro-active properties of the

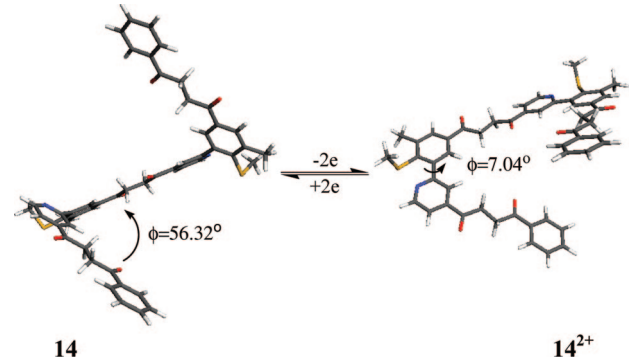

Figure 12. Open (reduced) and closed (oxidized) configurations of the proposed actuator constructed with two MMTPPy (**11**) hinges and three beams. The geometry optimization is at the B3LYP/6-31G(d) level.

MMTPPy unit are essentially unchanged in this multicomponent actuator. The torsion angle changes from around 56° to 7° for each unit, which corresponds to a strain value similar to that of the actuator **13**.

Conclusions

Molecular nanoactuators were designed on the basis of the electroactive molecules MSPPy (**3**) and MMTPPy (**11**) proposed in this study. The calculations indicate the formation of S∴N (sp^2) hemibonds in their one-electron oxidized states, which results in the planarization of the 2PPy scaffolds of the two molecules. The stretching frequency, molecular geometry, and MBO index suggest that the intramolecular S∴N (sp^2) hemibond strength is comparable to that of typical 2c/3e S∴X bond. The S∴N (sp^2) hemibond strength was estimated showing bonding energies around 18−22 kcal/mol. By introducing a methyl group ortho to the H_3CS- group in MSPPy (**3**), an even more effective actuating molecule, MMTPPy (**11**), is proposed. The methyl group functions as a directional block impairing the C−S···N interaction in the neutral state. The MMTPPy (**11**$^{\bullet+}$) displays a higher rotational barrier than MSPPy (**3**$^{\bullet+}$) along the bridge CC bond of the 2PPy pivot, which also makes it more suitable to function as electroactive materials. The molecular actuators were constructed by equipping the electroactive MMTPPy (**11**) with rigid beams.

The conformational change of the proposed electroactive biphenyl pivot is based on the formation of an SN hemibond and the first part of the presented material focuses on providing evidence for this. The difference in conformation occurs at different oxidation states, and forms the basis of the proposed actuation mechanism. This is different from atropisomers, where the conformation is maintained by steric effect. The key point of the proposed actuation is that the redox process drives the formation/dissociation of the SN hemibond, which in turn moves the equilibrium geometry between two different conformation of the two oxidation states.

The actuation simulations show that the proposed actuators exhibit a relatively large strain response of the order of 88%. More importantly, for the molecular actuators built with more than one MMTPPy (**11**) hinge,

each unit works independently but in unison in a redox process, and their motions jointly contribute to the actuating behavior of the nanoactuators.

Acknowledgment. Financial support from the National Science Foundation (Grant DMR-0331710) is gratefully acknowledged. Support by GridChem is acknowledged for computer time.

Supporting Information Available: Complete author list of ref 22, total energies and optimized geometries of **3**, **3**$^{\cdot+}$, **4**$^{\cdot+}$, **5**$^{\cdot+}$, **6**$^{\cdot+}$, **7**$^{\cdot+}$, **8**$^{\cdot+}$, **9**$^{\cdot+}$, **10**$^{\cdot+}$, **11, 11**$^{\cdot+}$, **12**$^{\cdot+}$, **13**, **13**$^{\cdot+}$, **14**, and **14**$^{\cdot+}$ (PDF). This material is available free of charge via the Internet at http://pubs.acs.org.

CM900029Z